PHYSICAL REVIEW C VOLUME 38, NUMBER 6 DECEMBER 1988

Neutral strange particle production and inelastic cross section in $\bar{p}$+Ta reaction at 4 GeV/c

K. Miyano and Y. Noguchi*
Department of Physics, Niigata University, Niigata 950-21, Japan

Y. Yoshimura, M. Fukawa, F. Ochiai,† T. Sato, R. Sugahara, A. Suzuki, and K. Takahashi
National Laboratory for High Energy Physics, KEK, Ibaraki 305, Japan

N. Fujiwara, S. Noguchi, and S. Yamashita
Department of Physics, Nara Women's University, Nara 630, Japan

A. Ono
College of Liberal Arts, Kobe University, Nada-ku, Kobe 657, Japan

M. Chikawa,‡ O. Kusumoto, and T. Okusawa
Department of Physics, Osaka City University, Osaka 558, Japan
(Received 29 February 1988)

The inclusive production of K_s^0, Λ, $\bar{\Lambda}$, and $K_s^0\Lambda$ in the $\bar{p}$Ta reaction at 4 GeV/c was measured and compared with that in the $\bar{p}p$ reaction. The total inelastic and topological cross sections were also measured. The number of Λ's produced in the $\bar{p}$Ta reaction was 11.3 times larger than that expected from the geometrical cross section, which is defined as $A^{2/3}$ times the cross section for the $\bar{p}p$ reaction. The yield ratio $\bar{\Lambda}/\Lambda$ was found to be 2×10^{-2}. These values cannot be accounted for by a straightforward extension of the $\bar{p}N$ reaction. Besides, a correlation of 2 vees like K_s^0-Λ could not prove their simultaneous production. Nuclear temperatures of 135 and 97 MeV were obtained from the kinetic energy spectra of K_s^0 and Λ, respectively. The kinematical characteristics of the K_s^0 and Λ produced were analyzed in terms of the fireball model.

I. INTRODUCTION

Recently, a considerable number of experimental studies have been performed on hadron-nucleus and nucleus-nucleus collisions in the GeV region in order to search for high-temperature and high nuclear density phenomena. In particular, strange particles have been observed extensively,[1-9] since it is expected that they can be detected as labeled particles useful for finding new nuclear reaction mechanisms at high temperatures. Some theories predict that the large yield of strange particles may be caused by a quark-gluon plasma.[10-15] Strange-particle production has also been analyzed regarding such reaction mechanisms as the multinucleon effect,[16] subthreshold production,[17] or the fireball model.[18,19] However, there have not been sufficient experimental data concerning strange-particle production to understand high-energy nuclear reactions.

Hadrons are preferable to heavy ions as projectiles for observing fundamental reaction dynamics. But, they have disadvantages for producing high temperatures in nuclei. With regard to this point, $\bar{p}$'s are useful owing to their large inelastic cross sections, including annihilation reactions. Besides, $\bar{p}$'s with energies of a few GeV may release their entire energies near the surface of a nucleus and heat up a tiny domain.[10,20] Such $\bar{p}$-induced nuclear reactions can be expected to produce new information concerning unusual phenomena. But, there have been only a few studies on strange-particle productions in high-energy, $\bar{p}$-induced nuclear reactions.[1] Therefore, we chose $\bar{p}$'s as projectiles and have studied the behavior of neutral strange-particle production in $\bar{p}$Ta reactions, while comparing this data with our previous data concerning $\bar{p}p$ reactions at 4 GeV/c.[21,22] A preliminary report of our results has been published.[23] In this paper the new results, including multiple vee events, are presented together with the measured total inelastic and topological cross sections.

II. EXPERIMENTAL PROCEDURE

A. $\bar{p}$ beam

Two Ta plates of 4.4 mm in thickness, Ta-1 and Ta-2, were installed in the KEK 1-m hydrogen bubble chamber, which was exposed to 4-GeV/c $\bar{p}$ beams. $\bar{p}$ beams were created by irradiating a Pt target with proton beams from the 12-GeV proton synchrotron at the National Laboratory for High Energy Physics, KEK. $\bar{p}$'s were separated from other negative particles by a 87-m double-stage beam channel, $K1$, which had two dc separators (9 and 6 m in length) and momentum-analyzing magnets. In front of an entrance window of the bubble chamber, a pressurized freon-12 gas Cherenkov counter was set in order to measure the $\bar{p}$ beam purity; a value of 98% was obtained. This value was confirmed by measuring the energy spectrum of knock-on electrons produced by beam particles in the bubble chamber.

B. Scanning and measuring

Fourteen thousand pictures were scanned to obtain a total inelastic cross section, topological cross sections, and charged particle multiplicities. Short prongs of less than 100 MeV/c were not counted in this scanning.

The events associated with vees were searched twice in 107 K pictures. The sensitivity was 5.02 events/mb. Ten thousand pictures were scanned three times by physicists in order to determine the scanning efficiency, which was 97%.

Tracks of the incident beams and vees were measured by manual image plane digitizers. The reaction positions inside the Ta plates were determined by interpolating charged secondary tracks and beams. This interpolation did not impair the quality of the analysis (as mentioned in succeeding sections). The measured events were processed by a reconstruction program called TVGP. Then, physicists judged the events as to whether remeasurement should be performed or not. Measurements were repeated three times for events which failed in reconstruction by TVGP. The vees of 97% could be successfully reconstructed and accepted in the analysis.

C. Particle identification

The invariant mass of the vees was examined by assuming decay tracks to be $\bar{p}$, p, π, or e in order to perform a mass cut. The p_t distribution was checked for all vees under the hypothesis $\gamma \to e^+e^-$, where p_t is the transverse momentum of a negative track with respect to the vee's momentum direction. Another criterion was the association angle θ_a; the angle between the direction connecting the reaction point with the vee vertex point and the direction of momentum of the vee (deduced by the decay tracks of the vee). We set the following cuts for the invariant mass, p_t, and θ_a:

(1) invariant mass hypothesis of the vee,

$$450 \text{ MeV} \le M(\pi^+\pi^-) \le 550 \text{ MeV for } K_s^0 ,$$

$$1100 \text{ MeV} \le M(\pi^-p) \le 1130 \text{ MeV for } \Lambda ,$$

$$1100 \text{ MeV} \le M(\pi^+\bar{p}) \le 1130 \text{ MeV for } \bar{\Lambda} ,$$

(2) p_t,

$$p_t \le 210 \text{ MeV}/c \text{ for } K_s^0 ,$$

$$p_t \le 110 \text{ MeV}/c \text{ for } \Lambda \text{ or } \bar{\Lambda} ,$$

(3) association angle,

$$\theta_a \le 10^\circ .$$

Finally, the bubble densities of the decay tracks and beams were compared with the TVGP results. The p's and $\bar{p}$'s tracks could be identified up to a momentum of 1.2 GeV/c. The γ's vee was easily removed from K_s^0, Λ, and $\bar{\Lambda}$ by the above cuts and bubble densities, since it had $p_t <$ a few MeV/c, an invariant mass <30 MeV, and a sharp vee shape with thin tracks.

We classified the vees into two grades according to the quality of particle identification. The first grade comprised vees which could be uniquely identified with above cuts and bubble densities; the second grade comprised vees which could be assigned to neither K_s^0 nor $\Lambda(\bar{\Lambda})$. The vees in the second grade had straight tracks that were too short or too fast, resulting in poor momentum measurements. The number of vees in the first grade was 1467; there was 125 in the second grade. In the following analysis we used only the vees of the first grade, which is given in Table I. The ambiguity in particle identification could be efficiently reduced by this classification. The measuring efficiencies were calculated as being 91 and 93 % for plate Ta-1 and Ta-2, respectively. The efficiency for Ta-1 in the upstream side was slightly lower than that for Ta-2 in the downstream side, since the decay track of a vee sometimes stuck Ta-2; thus its length became too short to measure its momentum.

Figure 1 shows a scatter plot of $M(\pi^-p)$ vs $M(\pi^+\pi^-)$, where the positive track is assumed to be π^+ or p. There are two distinctive bands corresponding to Λ and K_s^0 masses. Standard deviations of the measured mass were 30, 7.5, and 38 MeV for K_s^0, Λ, and $\bar{\Lambda}$, respectively. The comparatively large widths for K_s^0 and $\bar{\Lambda}$ masses were due to their high momentum in the laboratory system. The p_t distributions of π from K_s^0, Λ, and $\bar{\Lambda}$ are shown in Fig. 2. At $p_t = 200$ and 100 MeV/c prominent peaks can be seen which correspond to the kinematic boundaries of the K_s^0 and Λ decays. In the p_t spectrum for $\bar{\Lambda}$, a broad peak can also be seen around 100 MeV/c, in spite of the low statistics and high momentum. The angular distribution of π^- from the K_s^0 decay was also isotropic in the vee rest frame. It could thus be confirmed that the vees were assigned well to γ, K_s^0, Λ, and $\bar{\Lambda}$ and that the particle identification did not include any bias, although comparatively loose cuts were imposed.

D. Corrections

Each vee event was weighted by a factor $W(=1/p_r)$, where p_r is the probability for potentially observing the vee; it can be expressed as

$$p_r = \exp(-L_{\min}/L) - \exp(-L_{\max}/L) ,$$

where $L(=cp\tau/M)$ is the flight length of the vee, $L_{\max}$ the path length from the reaction point to the boundary of the fiducial volume, and $L_{\min}$ an observable minimum distance between the reaction point and the vee vertex. M, τ, and p are the mass, lifetime, and momentum of the vee.

Weighted values of K_s^0, Λ, and $\bar{\Lambda}$ were plotted as a function of the distance between the reaction point and the vee vertex. From the plot, $L_{\min}$ was established as 1.2 cm for K_s^0 and 1.6 cm for Λ. Since data of $\bar{\Lambda}$ had low statistics, the parameter $L_{\min}$ for Λ was also used for $\bar{\Lambda}$. These values of $L_{\min}$ were larger than those for the usual elementary reaction, because finding a vee near the reac-

TABLE I. Summary of number of events, measured cross sections, geometrical cross sections, and parameters n for K_s^0, Λ, and $\bar{\Lambda}$ productions in the $\bar{p}$Ta and $\bar{p}p$ reaction at 4 GeV/c.

Reaction	Number of events	Measured cross section (mb)	Geometrical cross section (mb)	n
$\bar{p}\text{Ta} \to K_s^0 X$	445	82.0±6.0	60.8	0.72±0.02
$\to \Lambda X$	929	193±12	17.0	1.13±0.02
$\to \bar{\Lambda} X$	21	3.8±2.0	15.4	0.42±0.09
$\to K_s^0 K_s^0 X$	17	4.0±1.0	9.6	0.50±0.05
$\to K_s^0 \Lambda X$	74	24.8±2.8	1.1	1.26±0.03
$\to K_s^0 \bar{\Lambda} X$	1	0.4±0.4	0.9	
$\to \Lambda \bar{\Lambda} X$	6	1.9±0.8	9.6	0.36±0.04
$\to \Lambda \Lambda X$	19	6.7±1.5		
$\to K^\circ \Lambda \Lambda X$	1	0.6±0.6		
$\to$inelastic		1628±30	2210	0.608±0.004
$\bar{p}p \to K_s^0 X$	2842	1.90±0.07		Ref. 21
$\to K_s^0 K_s^0 X$	246	0.30±0.02		Ref. 21
$\to \Lambda X$	757	0.53±0.05		Ref. 22
$\to \bar{\Lambda} x$	596	0.48±0.05		Ref. 22
$\to \bar{\Lambda} \Lambda X$	217	0.30±0.05		Ref. 22
$\to K_s^0 \Lambda X$	27	0.035±0.007		Ref. 22
$\to K_s^0 \bar{\Lambda} X$	10	0.014±0.005		Ref. 22
$\to$total		69		World data

tion point was difficult due to many secondary tracks. $L_{\min}$ for K_s^0 was smaller than those for Λ and $\bar{\Lambda}$, since the thinner decay tracks of K_s^0 could be easily distinguished from other thick secondary tracks. The average weights were 1.38 for K_s^0, 1.44 for Λ, and 1.43 for $\bar{\Lambda}$. Lifetimes $c\tau$ were deduced from the distributions of the decay length to be 2.8+0.3 cm for K_s^0 and 7.2±0.5 cm for Λ. These are in good agreement with world data. Vees which are emitted around 90° in the laboratory system were often absorbed in the Ta plates. This absorption was calculated to be about 16% by using their longitudinal momentum spectra in the laboratory system.

Corrections were made for (a) the limited detection volume by using the weight mentioned above, (b) scan-

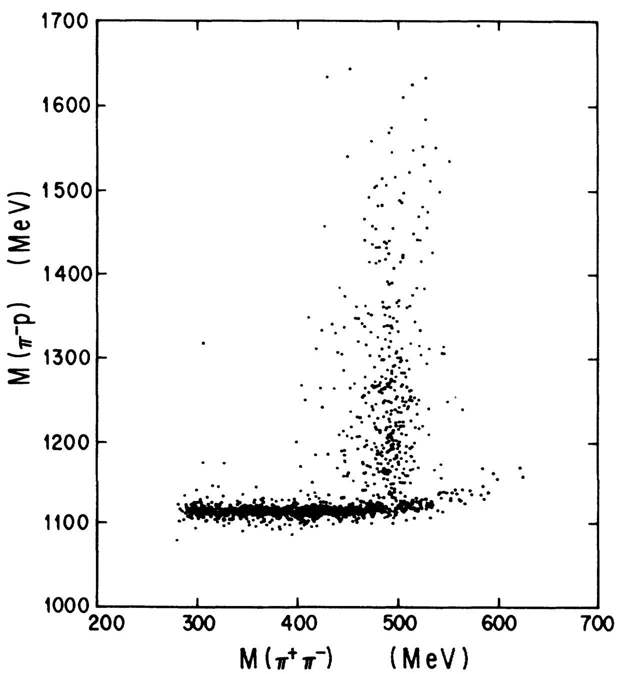

FIG. 1. Plot of the invariant mass for $M(\pi^- p)$ vs $M(\pi^+\pi^-)$ after cuts.

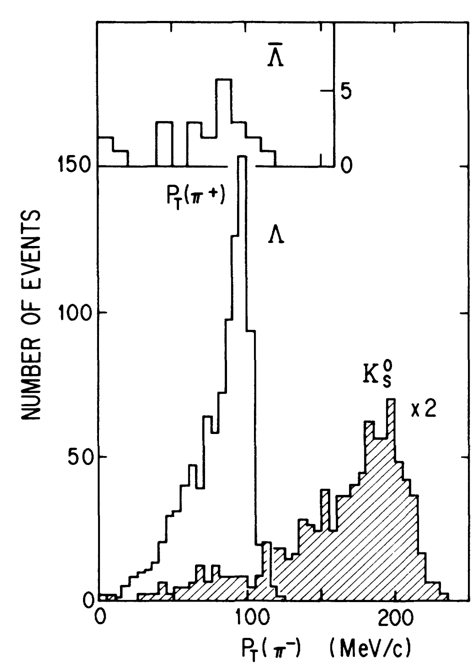

FIG. 2. p_t distributions of π^- from vees assigned to K_s^0, Λ, and $\bar{\Lambda}$. The hatched distribution is that of K_s^0.

ning loss (3%), (c) failure in identification of vees (8.5%), (d) absorption in the target plates (16%), and (e) unseen neutral decay modes.

III. EXPERIMENTAL RESULTS

A. Cross sections and multiplicities

The production cross sections for K_s^0, and Λ, and $\bar{\Lambda}$ are summarized in Table I, together with the results in $\bar{p}p$ at 4 GeV/c.[21,22] A total inelastic cross section for the $\bar{p}$Ta reaction was obtained as being 1628±30 mb. This value is almost equal to the geometrical cross section of a Ta nucleus, which is defined as $A^{2/3}$ times the cross section for the $\bar{p}p$ reaction. The mass number, A, is 181 for Ta. An attempt to express as $A^n \times \sigma_{\bar{p}p}$ (vee) was also done for the vee-production cross sections. Indice n's obtained are given in Table I. The K_s^0 production cross section is close to $\sigma_{\bar{p}p}(K_s^0)\times A^{2/3}$, while the Λ production is 11.3 times larger than $\sigma_{\bar{p}p}(\Lambda)\times A^{2/3}$. The $\bar{\Lambda}$ production was found to be suppressed approximately as $\frac{1}{4}$ times the geometrical cross section. The $\bar{\Lambda}/\Lambda$ production ratio was obtained as being $(2.0\pm1.0)\times10^{-2}$.

Semi-inclusive $K_s^0\Lambda X$ production is much larger than the geometrical cross section and the ratio is about 22. But, the $K_s^0K_s^0X$ production ratio is 0.4. The $\Lambda\bar{\Lambda}X$ event is also suppressed as $\frac{1}{5}$ times the geometrical cross section. In the $\bar{p}$Ta reaction 19 $\Lambda\Lambda X$ events were observed and the cross section was found to be three times larger than that of the $\Lambda\bar{\Lambda}X$ event.

The multiplicity of charged particles was studied for events with and without K_s^0 (or Λ). The mean multiplicities are summarized in Table II. Figure 3 shows the topological cross section. The most frequent multiplicity is 5 prongs and the mean multiplicity $\langle N_{ch}\rangle$ is 5.66±0.03, which is 1.9 times larger than the value of 3.04 in the $\bar{p}p$ reaction at 4 GeV/c. The multiplicity distributions of positive and negative charged particles are shown in Fig. 4. The mean multiplicity, $\langle N_-\rangle$, is nearly equal to the value in the $\bar{p}p$ reaction and most of negative particles are gray tracks with $\beta>0.5$. This may reflect the primary process, since negative particles are supposed to be π^-'s and pions are produced more rarely in the secondary process. The multiplicity distribution of positive particles is broad and quite different from that for negative particles. Positive particles are produced three times more frequently than the negative ones and the charge balance shifts toward the positive. But the charge balance is satisfactorily maintained among the gray tracks, which are conceived to be π and the mean multiplicity ratio of the negative particles to the positive ones is 1.3±0.1. These values can be explained by taking the proton-neutron ratio in Ta nucleus into consideration.

TABLE II. Average charged particle multiplicities.

	Events without K_s^0 or Λ	Gray tracks	Events with K_s^0	Events with Λ
$\langle N_{ch}\rangle$	5.66±0.03	2.3±0.1	5.14±0.03	5.66±0.03
$\langle N_+\rangle$	4.33±0.03	1.0±0.1	3.90±0.02	4.52±0.02
$\langle N_-\rangle$	1.44±0.04	1.3±0.1	1.25±0.03	1.13±0.03

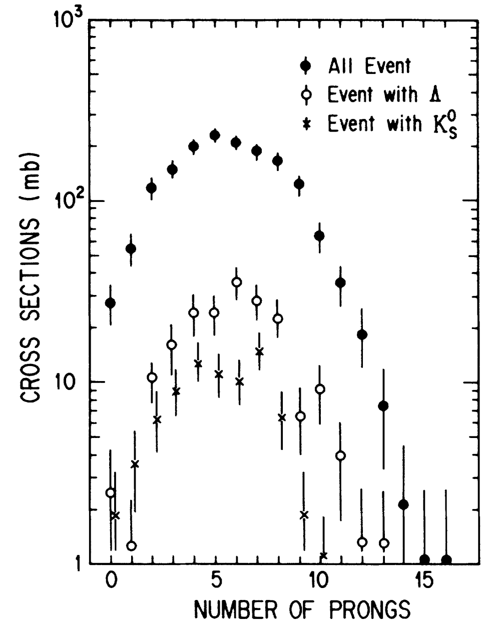

FIG. 3. Topological cross sections in the $\bar{p}$Ta reaction at 4 GeV/c.

As for events accompanied with K_s^0 or Λ, the multiplicity distributions do not differ from those for events without K_s^0 or Λ, as shown in Figs. 3 and 4. The mean multiplicities, $\langle N_-\rangle$, for events with K_s^0 or Λ are slightly smaller than those of events without K_s^0 or Λ, as given in Table II. Figure 5(a) shows the mean transversal momentum, $\langle p_T\rangle$, of K_s^0 and Λ as a function of the number of prongs. The mean rapidity, $\langle Y_1^*\rangle$, is given in Fig. 5(b). When the number of prongs increases, $\langle p_T\rangle$ and $\langle Y_1^*\rangle$ of K_s^0 become lower; but those of Λ do not significantly change with the number of prongs.

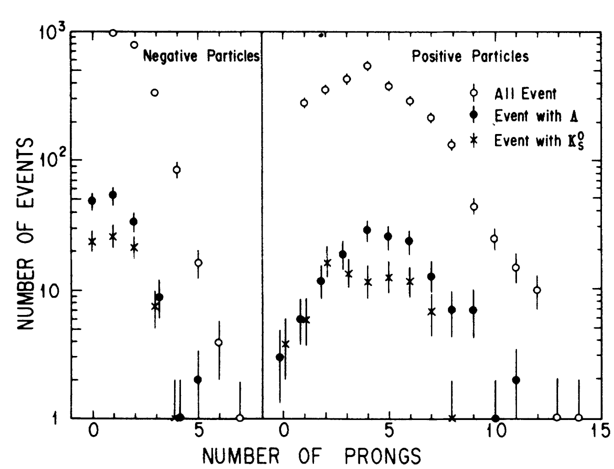

FIG. 4. Multiplicity distributions of positive and negative charged particles.

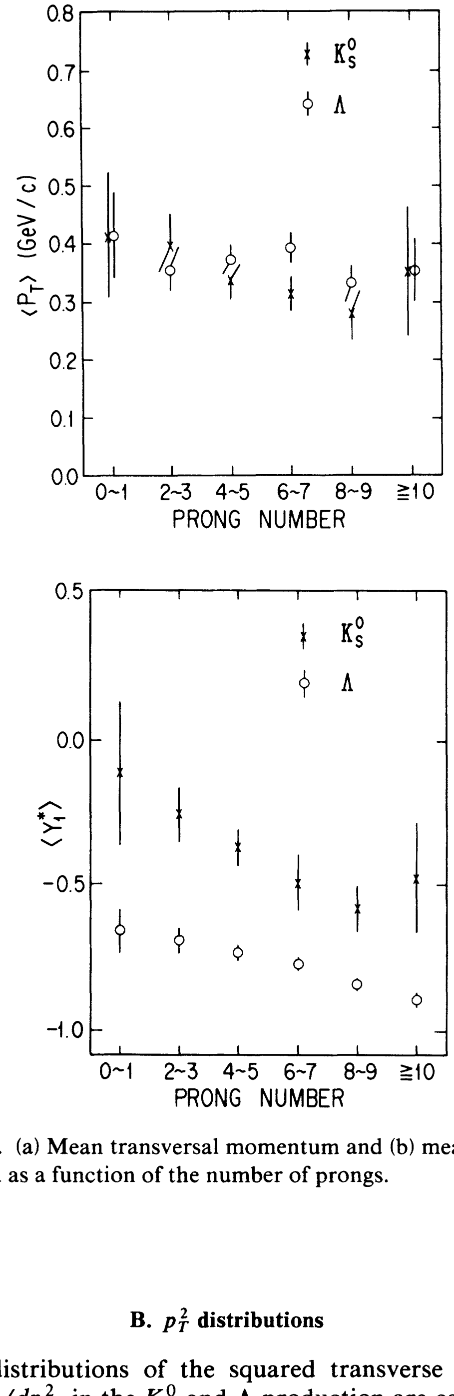

FIG. 5. (a) Mean transversal momentum and (b) mean rapidity plotted as a function of the number of prongs.

B. p_T^2 distributions

The distributions of the squared transverse momentum, $d\sigma/dp_T^2$, in the K_L^0 and Λ production are calculated and displayed in Fig. 6. The distributions were fitted to exponential functions, $d\sigma/dp_T^2 = A\exp(-Bp_T^2) + C\exp(-Dp_T^2)$. The values of the parameters, $A-D$, are given in Table III, together with those obtained in the $\bar{p}p$ reaction. The parameter D for $\bar{\Lambda}$ was not deduced because of low statistics. The B parameters (and D's) in the $\bar{p}$Ta reaction have almost the same values for the three cases of K_s^0, Λ, and $\bar{\Lambda}$. Also, these values are almost equal to those for Λ in the $\bar{p}p$ reaction. The ratio of A/C for K_s^0 and Λ is about 3 in the $\bar{p}$Ta reaction, while the ratio in the $\bar{p}p$ reaction is less than 1. Namely, the low p_T component in $\bar{p}$Ta is more dominant than that in the $\bar{p}p$ reaction.

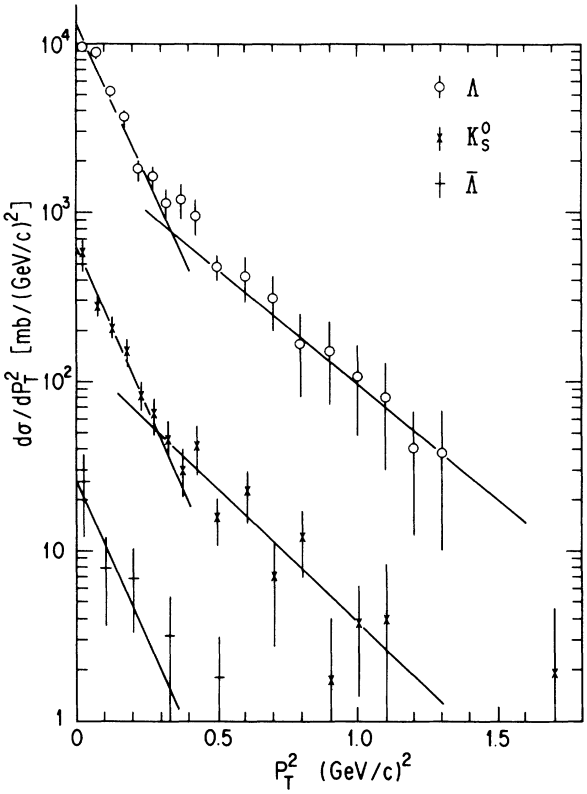

FIG. 6. $d\sigma/p_T^2$ spectra of K_s^0, Λ, and $\bar{\Lambda}$.

C. Rapidity and angular distributions

Figure 7 shows a rapidity distribution, $d\sigma/dy$, for K_s^0 in the $\bar{p}$Ta reaction. Y_1^* is the rapidity in the $\bar{p}-N$ center-of-mass system. The subscript (1) indicates the effective number of nucleons which makes the c.m. system with the incident $\bar{p}$. The solid curve represents the rapidity distribution for K_s^0 in $\bar{p}p$ at 4 GeV/c, which is magnified by the factor $A^{2/3}$. The shapes and magnitude of the distributions resemble each other very closely, but the positions of their peaks are different. The peak changes to 0 ($Y_3^* = 0$) and the distribution agrees with that for K_s^0 in $\bar{p}p$, if one takes the $\bar{p}-3N$ c.m. frame for $\bar{p}$Ta, i.e., that the incident $\bar{p}$ interacts with an effective target of three-nucleon mass which is moving at a velocity of $\beta=0.54$ in the laboratory system. Figure 8 shows the angular distribution of K_s^0 from the $\bar{p}\text{Ta}\to K_s^0X$ reaction in the $\bar{p}-3N$ c.m. frame. Although this angular dis-

TABLE III. Parameters of $d\sigma/dp_T^2 = A\exp(-Bp_T^2) + C\exp(-Dp_T^2)$.

Particle	A/C	B (GeV/c)$^{-2}$	D (GeV/c)$^{-2}$	Reference
$\bar{p}\text{Ta}\to K_s^0X$	2.8±0.6	8.4±0.4	2.1±1.5	
$\to\Lambda X$	2.7±0.3	7.3±0.4	3.4±1.0	
$\to\bar{\Lambda}X$		8.1±2.8		
$\bar{p}p\to K_s^0X$	0.88±0.08	14.1±1.0	4.8±0.1	21
$\to\Lambda X$	0.6±0.1	8.3±0.1	3.8±1.0	22

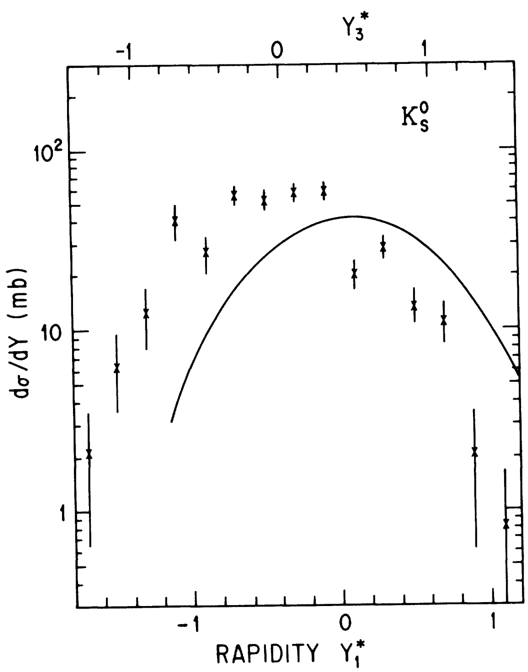

FIG. 7. Rapidity distribution of K_s^0. The solid curve shows the rapidity distribution of K_s^0 in $\bar{p}p$ interaction. Y_1^* and Y_3^* are defined in the $\bar{p}-N$ and $\bar{p}-3N$ c.m. frame, respectively.

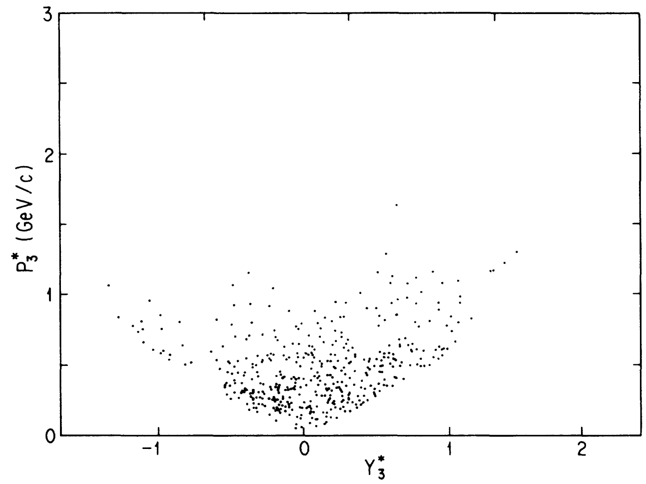

FIG. 9. Scatter plot of momentum p_3^* and rapidity Y_3^* of K_s^0 in $\bar{p}-3N$ c.m. frame.

tribution is dominant in the forward region in the $\bar{p}-N$ c.m. frame, it changes to a symmetric shape, like that of the $\bar{p}p$ reaction by taking the $\bar{p}-3N$ c.m. frame. Further, a scatter plot of p_3^* vs Y_3^* was made for K_s^0, where p_3^* was the momentum of K_s^0 in the same frame. The plot is symmetric for the point $Y_3^*=0$, and p_3^* reaches 0 at that point (Fig. 9).

A rapidity distribution of Λ in the $\bar{p}$Ta reaction is shown in Fig. 10. The distribution for Λ from $\bar{p}p$ at 4 GeV/c is also given by a solid curve, which is magnified by $A^{2/3}$. The peak lies at $Y_1^*=-0.82$ in the $\bar{p}-N$ c.m. frame; it changes to $Y_{13}^*=0$ in the $\bar{p}-13N$ c.m. frame with $\beta=0.24$. The width at half-maximum of the rapidity distribution is 0.6 and corresponds to a longitudinal momentum spread of ±340 MeV/c. This value is almost equal to the average transverse momentum of $\langle p_T\rangle=315$ MeV/c for Λ in region S (defined later), while $\langle p_T\rangle$ for all Λ was 370 MeV/c. In order to explore the rapidity distribution for Λ from $\bar{p}$Ta in further detail, a scatter plot of $p_{13}^*-Y_{13}^*$ was made (Fig. 11). Since most of the data points are concentrated in the region $p_{13}^*\leq 0.8$

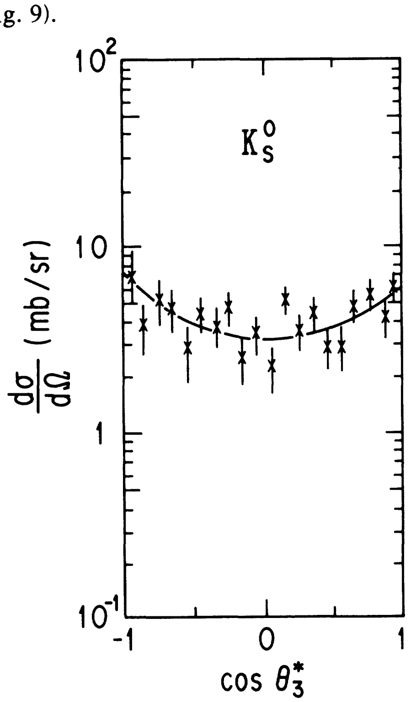

FIG. 8. Angular distribution of K_s^0 from the $\bar{p}$Ta$\rightarrow K_s^0X$ reaction in the $\bar{p}-3N$ c.m. frame. A solid line shows the $\bar{p}p\rightarrow K_s^0X$ reaction in the $\bar{p}-N$ c.m. frame, magnified by $A^{2/3}$.

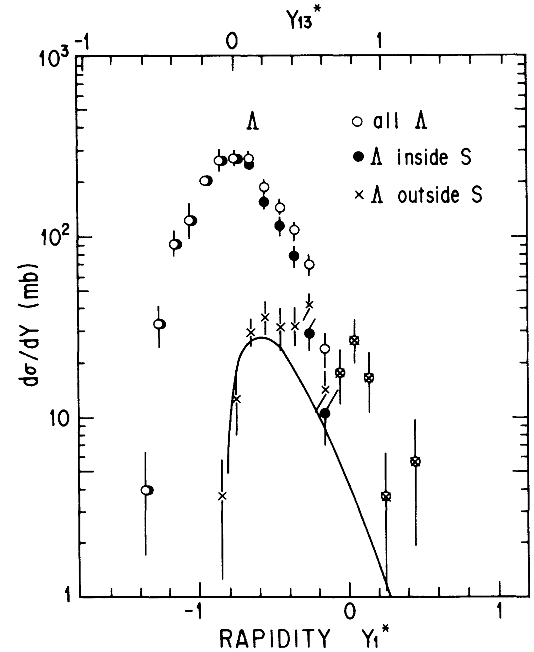

FIG. 10. Rapidity distribution of Λ. A solid curve shows the rapidity distribution of Λ in $\bar{p}p\rightarrow\Lambda X$ at 4 GeV/c, but it is magnified with a factor of $A^{2/3}$. See text concerning region S.

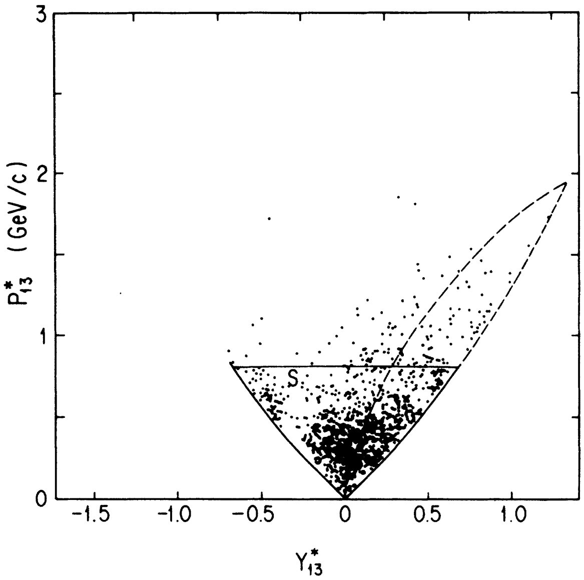

FIG. 11. Scatter plot of momentum p^*_{13} vs rapidity Y^*_{13} of Λ from $\bar{p}$Ta in the $\bar{p}-13N$ c.m. frame. The distribution of Λ from $\bar{p}p$ at 4 GeV/c is shown by the dashed curve.

GeV/c, we designate this region as S. Lack of data points at $Y^*_{13}=-0.25$ is attributed to absorption by target plates. The data points are distributed symmetrically about $Y^*_{13}=0$; the minimum of p^*_{13} also goes to 0 there. The dashed line indicates the region of the main part of Λ from the $\bar{p}p$ reaction in the same frame which is shifted by $Y^*_1=-0.82$. This region agrees considerably well with the data points outside region S.

In Fig. 10, the rapidity distribution of the data points in region S is reproduced by a Gaussian function: $\exp(-Y^{*2}_{13}/0.12)$. The data points outside region S fall in the higher tail of the rapidity distribution and corresponds well to the shape and magnitude of the distribution of Λ from $\bar{p}p$ at 4 GeV/c. The Λ production cross section inside region S can be expressed by using $\sigma_{\bar{p}p}(\Lambda)\times A^{1.08}$ and contributes to an enhancement of the Λ production yield in $\bar{p}$Ta. But, the cross section of Λ outside region S is $\sigma_{\bar{p}p}(\Lambda)\times A^{0.74}$ and is almost equal to the geometrical A dependence, $A^{2/3}$. The production ratio for these Λ's is about 6:1.

The angular distribution of all Λ's in the $\bar{p}-13N$ c.m. frame is displayed in Fig. 12(a). We could not obtain a symmetric angular distribution about $\cos\theta^*=0$ by changing the effective target mass. If we pick up only the Λ's in region S, these Λ's have almost an isotropic angular distribution, indicating the evaporation character of the production process [Fig. 12(b)]. On the other hand the Λ's outside region S are dominant in the forward region in the $\bar{p}-13N$ c.m. frame. When one takes the $\bar{p}-N$ c.m. frame, the angular distribution becomes dominant in the backward region, which is similar to that of Λ from $\bar{p}p$ [Fig. 12(c)]. Its magnitude is also almost equal to the value obtained from $\bar{p}p$ by magnifying by $A^{2/3}$.

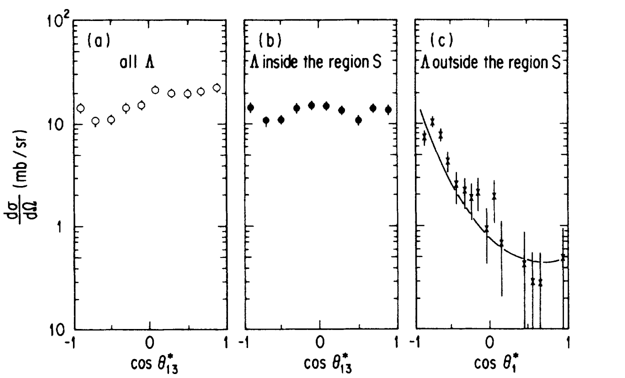

FIG. 12. Angular distribution of Λ. (a) All Λ in the $\bar{p}-13N$ c.m. frame, (b) Λ in the region S in the $\bar{p}-13N$ c.m. frame, and (c) Λ outside the region S in $\bar{p}-N$ c.m. frame. The solid curve is the angular distribution of Λ from $\bar{p}p$, magnified by $A^{2/3}$.

D. Scatter plot of rapidity vs transverse momentum

$Y^*_1-p_T$ scatter plots for K^0_s and Λ from the $\bar{p}$Ta reaction are made as shown in Fig. 13. The solid curves represent the kinematical boundaries for K^0_s and Λ production in elementary processes $\bar{p}N\to K^0_sK$ and $\Lambda\bar{\Lambda}$ at 4 GeV/c, respectively. Since the boundaries of the other production reactions, like $\bar{p}N\to K^0_s\Lambda\bar{N}$, should lie within these solid curves, these curves express the widest boundaries for K^0_s and Λ produced in elementary processes.

All data points for K^0_s fall uniformly inside the kinematical boundary, whereas about half of the points

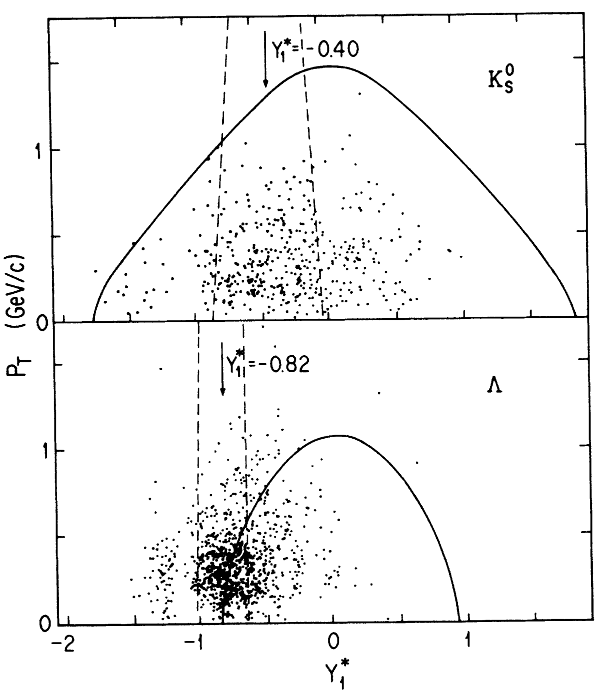

FIG. 13. Scatter plots of $Y^*_{13}-p_T$. Solid curves show kinematical limits in $\bar{p}N\to K^0_sK^0_s$ and $\bar{p}N\to\Lambda\bar{\Lambda}$. Dashed curves give limits in the $\bar{p}-3N$ c.m. frame for K^0_s and the $\bar{p}-13N$ c.m. frame for Λ. Arrows show the centers of the rapidity distributions.

for Λ lie outside the lower boundary of rapidity. When one takes the $\bar{p}-13N$ c.m. frame for Λ production and if the effective target is a solid lump of 13 nucleons, a new region is defined with a new boundary shown by dotted lines in Fig. 13. In this case one should observe Λ's with very high P_T ($P_{T\,\max}=3.1$ GeV/c). The observed Λ's, however, are concentrated in the region of low p_T. Although these circumstances are similar to K_s^0, Λ production is affected more significantly by the evaporation character than that of K_s^0. Harris *et al.*[2] have also observed in heavy-ion reactions that most of the Λ's are beyond the kinematical boundary of the $NN\rightarrow\Lambda KN$ reaction at 1.8 GeV, indicating the necessity of collective multiparticle interactions.

E. Semi-inclusive production

The semi-inclusive production of $K_s^0K_s^0$ and $K_s^0\Lambda$ was analyzed. The rapidity and the angular distribution are shown in Figs. 14 and 15. It can be seen from the figures that the rapidity and angular distributions of Λ's from $K_s^0\Lambda X$ events are similar to those for the above-stated inclusive production. Although the rapidity distribution of K_s^0's from the $K_s^0\Lambda X$ event shifts to the lower side, compared with Fig. 7, the shape is much the same when considering the contribution of the $K_s^0K_s^0X$ event.

By supposing the following processes in a Ta nucleus for the $K_s^0\Lambda$ semi-inclusive productions,

$$\bar{p}N\rightarrow XX',$$

$$XN\rightarrow K_s^0\Lambda\ ,$$

the invariant mass and momentum of intermediate matter, X, could be calculated; their distributions are given in Fig. 16. The concentrated mass distribution at 1.9 GeV is a surprising result. If one assumes the above-mentioned process, it is difficult to attribute X to π or $\bar{K}$. It seems, rather, that the $K_s^0\Lambda$ are produced by reactions between a $(N\bar{N})$ pair and another nucleon. But, such a reaction could not simultaneously simulate two experimental results that the rapidity distribution of Λ's is concentrated around $Y_{13}^*=0$ and that the angular distribution is isotropic in the $\bar{p}-13N$ c.m. frame. These distributions can be reproduced by assuming that K_s^0 and Λ are produced individually in secondary interactions or are multiscattered in the target nucleus before these par-

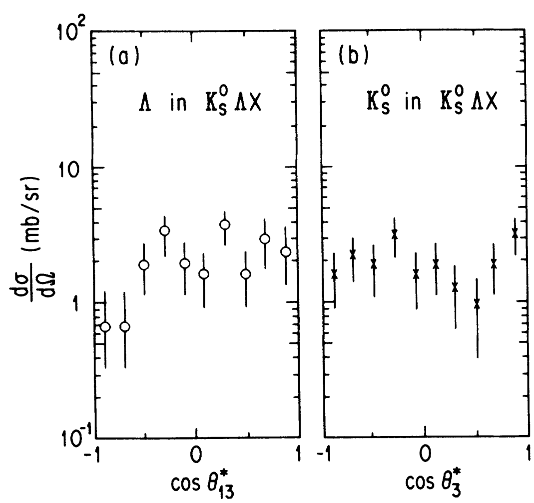

FIG. 15. Angular distribution of K_s^0 and Λ from the $\bar{p}\mathrm{Ta}\rightarrow K_s^0\Lambda X$ reaction.

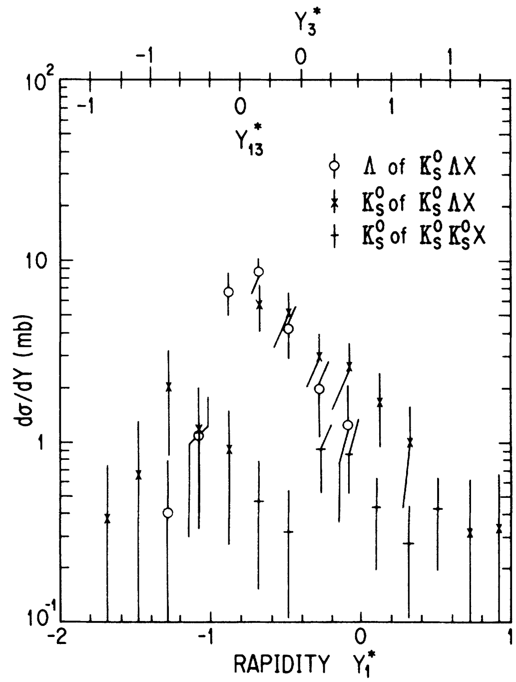

FIG. 14. Rapidity distribution of K_s^0 and Λ from the $\bar{p}\mathrm{Ta}\rightarrow K_s^0\Lambda X$ and $K_s^0K_s^0X$ reaction.

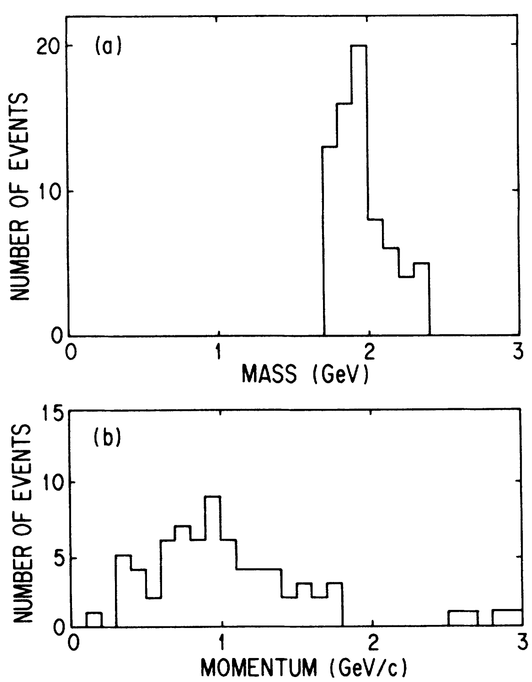

FIG. 16. Invariant mass and momentum of intermediate matter, X, in the assumed $\bar{p}N\rightarrow XX'$, $XN\rightarrow K_s^0\Lambda$ processes for the $K_s^0\Lambda X$ semi-inclusive production.

ticles are emitted, since there is not any correlation between K_s^0 and Λ. Such assumptions are supported by our observation that the rapidity of K_s^0's and Λ's are not correlated with each other.

F. Nuclear temperature

Until now, high nuclear temperatures have been observed in terms of the energy spectra of particles produced in nuclear reactions over a wide range of incident energy. But, temperatures have been defined in various frames, i.e., those defined in the laboratory system and others in moving frames. We have defined temperatures in the moving frames, which are the $\bar{p}-3N$ c.m. frame with a velocity $\beta=0.54$ and the $\bar{p}-13N$ c.m. frame with $\beta=0.24$ for K_s^0 and Λ, respectively. The invariant cross section is described by a simple exponential formula,

$$\frac{E^*}{p^{*2}}\frac{d^3\sigma}{dp\,d\Omega}=\text{const}E^*\exp(-T^*/\theta^*)\ ,$$

where E^* is the total energy and T^* the kinetic energy of the K_s^0 or Λ in each c.m. frame.

Figure 17 shows the spectra of the invariant production cross sections of K_s^0 and Λ as a function of each kinetic energy, T^*. The solid lines for K_s^0 and Λ are inverse parameters, θ, of 135 ± 13 and 97 ± 6 MeV, respectively. The large deviation of data of the Λ's from the line in the high-energy region is due to the Λ's found outside region S (described above). These values observed in the present experiment are still far too low in terms of the critical temperature required for a phase transition to the quark-gluon plasma, except for another recent estimation.[24]

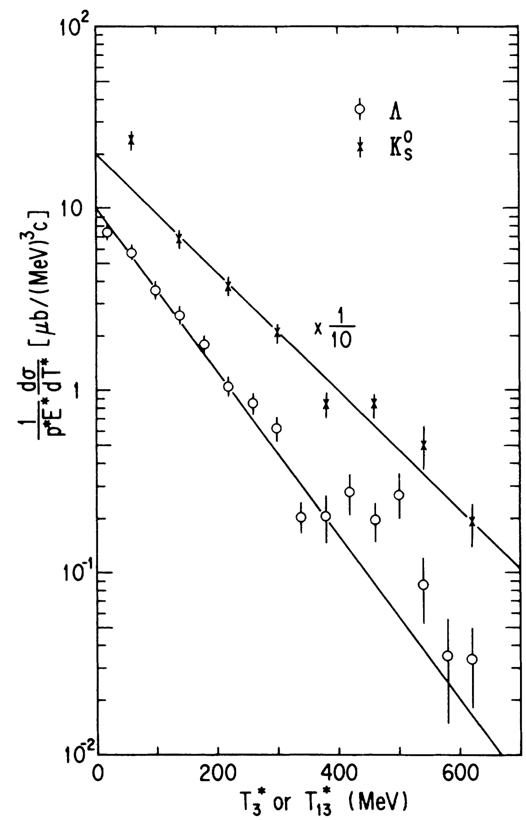

FIG. 17. Spectra of the kinetic energy T^* of K_s^0 of Λ. T^* of K_s^0 is kinetic energy in the $\bar{p}-3N$ c.m. frame. T^* of Λ is defined in the $\bar{p}-13N$ c.m. frame. Solid lines have inverse slope parameters of 135 MeV for K_s^0 and 97 MeV for Λ, respectively.

G. Polarization of Λ

The polarization of Λ from the $\bar{p}$Ta reaction was measured through the weak decay to p and π^-. The polarization P was calculated by using

$$P=\frac{3}{\alpha N}\sum_{i=1}^{N}q_i n_i\ ,$$

where N is the total number of observed Λ decays. q_i is a unit vector along the flight direction of the proton in the Λ rest frame. n_i is a unit vector normal to the production plane containing the momenta of a beam and a produced Λ: namely, $n_i=(q_b\times q_\Lambda)/|q_b\times q_\Lambda|$, where q_b and q_Λ are the momenta of the beam and Λ, respectively. The decay symmetry parameter, α, is taken as 0.642 from the particle data table.

Figure 18 shows the polarization of Λ as a function of p_T together with published data.[25–27] We estimated the systematic error by measuring the polarization of K_s^0 decaying to π^+ and π^-. The estimated systematic error was much smaller than the statistical uncertainty of the data. Thus, only the statistical uncertainty is quoted. The polarization obtained in the present experiment does not change with p_T and the average polarization was 0.02 ± 0.09.

IV. DISCUSSION

In this experiment, the total inelastic cross section was almost equal to the geometrical value. This is reasonable, since an elastic $\bar{p}N$ collision inside a Ta nucleus must often result in breaking the nucleus. The cross section of K_s^0 production was also nearly equal to the geometrical

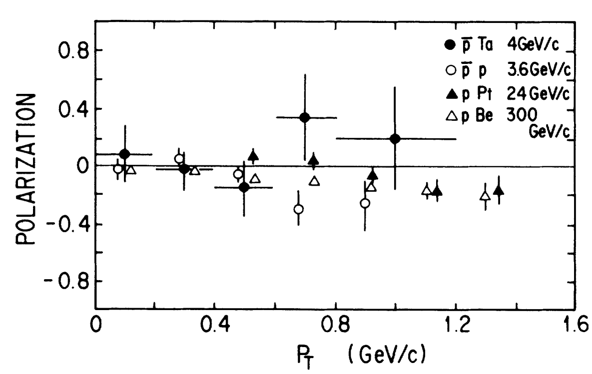

FIG. 18. Polarization of Λ.

value. But, a larger Λ production yield and a very small $\bar{\Lambda}$ yield cannot be expected in terms of the geometrical cross section. Similar trends have been observed even in $\bar{p}d$ reactions at the energy region between 0.55 and 2.9 GeV/c.[28-31] The importance of secondary interactions of kaon, $\bar{p}$, and $\bar{\Lambda}$ in the target nucleus has been pointed out by several authors.[30-33]

We tried to estimate the contribution of secondary interactions in Λ production. The most likely source of Λ is a secondary interaction between the $\bar{K}$ produced in the reaction $\bar{p}N \rightarrow K\bar{K}X$ and the surrounding nucleons in the Ta nucleus. We write the cross section as

$$\sigma_K(\bar{p}\mathrm{Ta} \rightarrow K\bar{K}X \rightarrow K\Lambda X) = \sigma(\bar{p}\mathrm{Ta} \rightarrow K\bar{K}X) \times \mathrm{probability}(\bar{K}N \rightarrow \Lambda X)$$
$$= A^{2/3}\sigma(\bar{p}N \rightarrow K\bar{K}X) \times \mathrm{probability}(\bar{K}N \rightarrow \Lambda X) ,$$

where

$$\mathrm{probability}(\bar{K}N \rightarrow \Lambda X) = \rho\sigma(\bar{K}N \rightarrow \Lambda X)\langle R \rangle .$$

The $K\bar{K}X$ production cross section in the $\bar{p}$Ta reaction is calculated assuming that the $\bar{K}$'s are produced with a ratio of the geometrical cross section. The cross section $\sigma(\bar{p}N \rightarrow K\bar{K}X)$ is deduced to be about 5 mb from the value for the reaction $p\bar{p} \rightarrow K_s^0 K_s^0 X$ at 4 GeV/c (0.30 mb), supposing that all $K\bar{K}$ pair combinations are equally produced in the $\bar{p}p$ reaction:

$$\sigma(K^+K^-) = \sigma(K^+K^0) = \sigma(K^0K^-) = \sigma(K^0K^0)$$

and

$$\sigma(K_s^0K_s^0) = \sigma(K_L^0K_s^0) = \sigma(K_s^0K_L^0) = \sigma(K_L^0K_L^0) .$$

Probability $(\bar{K}N \rightarrow \Lambda X)$ is about 0.5 by using 6 mb as the average cross section for the $\bar{K}N \rightarrow \Lambda X$ and $\rightarrow \Sigma^0 X$ reactions, 0.17 nucleons/fm^3 for a nuclear density ρ and 5 fm for the effective mean nuclear radius $\langle R \rangle$. Then, $\sigma_K(\bar{p}\mathrm{Ta} \rightarrow K\bar{K}X \rightarrow K\Lambda X)$ turns out to be about 75 mb.

In the same manner, $\sigma_\pi(\bar{p}\mathrm{Ta} \rightarrow \pi X \rightarrow K\Lambda X)$ was roughly estimated to be about 80 mb. The excess of Λ production above the geometrical cross section is almost attributed to be the sum of $\sigma_K(\bar{p}\mathrm{Ta} \rightarrow K\bar{K}X \rightarrow K\Lambda X)$ and $\sigma_\pi(\bar{p}\mathrm{Ta} \rightarrow \pi X \rightarrow K\Lambda X)$. It seems reasonable that most of the Λ's are produced by secondary interactions. A quarter of the K_s^0's or a half of the $\bar{K}$'s produced in primary collisions of $\bar{p}$ must be spent by the secondary interaction to produce Λ's. On the other hand, some of the K_s^0's finally observed are considered to be also produced by secondary interactions. The number of the K_s^0's, however, are not observed as much as one estimates. A similar tendency can be seen for the $\bar{p}\mathrm{Ta} \rightarrow K_s^0\Lambda X$ reaction, though the observed cross section is very large compared with the geometrical cross section. By using 24.8 mb for the $\bar{p}\mathrm{Ta} \rightarrow K_s^0\Lambda X$ reaction, the cross section of $\bar{p}\mathrm{Ta} \rightarrow K\Lambda X$ can be estimated to be about 100 mb, including K_L^0 and K^+. But the value is half of the cross section observed in $\bar{p}\mathrm{Ta} \rightarrow \Lambda X$, notwithstanding the expectation that most of the Λ's are produced along with the K's.

Gibbs[34] has calculated the strangeness balance in the $\bar{p}$Ta reaction at 4 GeV/c and obtained a K_s^0/Λ yield ratio of 0.41, which agrees well with the present value of 0.42. The author also estimated the probability for $s\bar{s}$ quark formation in consideration of secondary interactions and found a probability of 0.15 per the $\bar{p}$ annihilation, which corresponds to 0.16 from our data. Recently, Ko and Yuan[35] have also studied the contributions of the secondary particles to Λ production on the $\bar{p}$Ta reaction in detail and obtained a production cross section of 122 mb, compared with our value of 193 mb. They emphasized that multiple scattering, including the nucleon cluster effect, should be investigated concerning the difference between these values before considering a quark-gluon plasma.

V. CONCLUDING REMARKS

In the $\bar{p}$Ta reaction we have obtained the total inelastic cross section and the topological cross sections, which were comparable to the geometrical values. The very large yield of Λ's and the suppressed yield of $\bar{\Lambda}$'s have been found. In order to explain the rapidity and angular distributions of K_s^0 and Λ production, heavy effective targets were required. But, the p_T spectra for K_s^0's and Λ's proved that these effective targets are soft lumps. Thus, a reasonable mechanism for K_s^0 and Λ production may be as follows: a leading particle from the primary reaction releases its energy through short-range correlations and the secondary particles continually increase through successive interactions, while the hot region expands in the target nucleus. The secondary particles move, as a whole, along the direction of incident $\bar{p}$, emitting K_s^0, Λ, and so on. K_s^0 comes out of the nucleus before the incident energy spreads in the nucleus, while most of the Λ's are emitted through evaporation-like behavior. Such a mechanism[36] has also been confirmed in terms of the following facts: (1) the angular distributions of K_s^0 and most of the Λ's are isotropic in the $\bar{p}-3N$ frame with $\beta=0.54$ and the $\bar{p}-13N$ frame with $\beta=0.24$, respectively, (2) the polarization of Λ is practically 0, and (3) the temperatures are 135 MeV for K_s^0 and 97 MeV for Λ. But, it is beyond comprehension by this mechanism why the mean multiplicity of negative particles is almost equal to the value in the $\bar{p}p$ reaction, since many π^- can be produced in secondary interactions. Also, the smallness of the observed cross sections for the $\bar{p}\mathrm{Ta} \rightarrow K_s^0\Lambda X$ reaction is not presently well explained. In this connection, further experimental studies should be performed, especially concerning $\bar{p}A \rightarrow K_s^0\Lambda X$ and $K^+\Lambda X$ for various nucleides and incident energies, to study the $\bar{p}$-nucleus reaction mechanism causing the extraordinary Λ yield.

The authors are thankful to K. Arimori and N. Arakawa for their contributions involving the analyses.

*Present address: Graduate School of Science and Technology, Kobe University, Kobe 657, Japan.
†Present address: Department of Liberal Arts, Tezukayama University, Nara 631, Japan.
‡Present address: Research Institute for Science and Technology, Kinki University, Higashiosaka 558, Japan.

[1]J. E. Elias, W. Busza, C. Halliwell, D. Luckey, P. Swartz, L. Votta, and C. Yound, Phys. Rev. D **22**, 13 (1980).
[2]J. W. Harris, A. Sandoval, R. Stock, H. Stroebele, R. E. Renfordt, J. V. Geaga, H. G. Puch, L. S. Schroeder, K. L. Wolf, and A. Dacal, Phys. Rev. Lett. **47**, 229 (1981).
[3]A. Shor, K. Ganezer, S. Abachi, J. Carroll, J. Geaga, G. Igo, P. Lindstrom, T. Mulera, V. Perez-Mendez, A. Sagle, D. Woodard, and F. Zarbakhsh, Phys. Rev. Lett. **48**, 1597 (1982).
[4]S. Schnetzer, M.-C. Lemaire, R. Lombard, E. Moeller, S. Nagamiya, G. Shapiro, H. Steiner, and I. Tanihata, Phys. Rev. Lett. **49**, 989 (1982).
[5]M. Anikina, M. Gazdzicki, A. Golokhvastov, L. Goncharova, K. Iovchev, S. Khorozov, E. Kuznetzova, J. Lukstins, E. Okonov, T. Ostanievich, S. Sidbrin, G. Vardenga, O. Balea, N. Nikirovich, T. Ponta, L. Chkhaidzer, T. Dzobava, M. Despotashvili, I. Tuliani, E. Khusaimov, N. Nurgozin, B. Suleimenov, E. Skerzypczak, and T. Tymieniecka, Phys. Rev. Lett. **50**, 1971 (1983).
[6]M. Anikina, V. Aksinenko, E. Dementiev, M. Gazdzicki, N. Glagoleva, A. Golokhvastov, L. Goncharova, A. Grachov, K. Iovchev, S. Kadykova, N. Kaminsky, S. Khorozov, E. Kuzunetsova, J. Lukstins, A. Matyushin, V. Matsyushin, E. Okonov, T. Ostanevich, E. Shevchenko, S. Sidorin, G. Vardenga, O. Balea, N. Nilorovich, T. Ponta, L. Chkhaidze, T. Dzobava, M. Destpotashvili, I. Tuliani, E. Khusainov, N. Nurgozin, B. Suleimanov, E. Skrzypczak, and T. Tymieniecka, Z. Phys. C **25**, 1 (1984).
[7]M. G. Abreu, T. Armstrong, M. Baubillier, W. Beusch, A. Burns, N. Erschaidat, J. Gago, A. Jacholkowski, K. Knudson, S. Otwinowski, D Perrin, A. Palano, M. Pimenta, E. Quercigh, Z. Strachman, M. Szeptycka, S. Tkaczyk, R. Walczak, and R. Zitoun, Z. Phys. C **25**, 115 (1984).
[8]E. Barasch, A. Shor, S. Abachi, J. Carroll, P. Fisher, K. Ganezer, G. Igo, T. Mulera, V. Perez-Mendez, and S. Trentalange, Phys. Lett. **161B**, 265 (1985).
[9]F. Balestra, M. P. Bussa, L. Busso, L. Fava, L. Ferrero, D. Panzieri, G. Piragino, F. Tosello, G. Bendiscioli, A. Rotondi, P. Salvini, A. Zenoni, Yu. A. Batusov, I. V. Falomkin, G. B. Pontecorvo, M. G. Sapozhnikow, V. I. Tretyak, C. Guaraldo, A. Maggiora, E. Lodi Rizzini, A. Haatuft, A. Halsteinslid, K. Myklebost, J. M. Olsen, F. O. Breivik, T. Jacobsen, and S. O. Sorensen, Phys. Lett. B **194**, 192 (1981).
[10]J. Rafelski, Phys. Lett. **91B**, 281 (1980).
[11]J. Rafelski and B. Müller, Phys. Rev. Lett. **48**, 1066 (1982).
[12]T. S. Biro and J. Zimanyi, Nucl. Phys. **A395**, 525 (1983).
[13]P Koch, J. Rafelski, and W. Greiner, Phys. Lett. **123B**, 151 (1983).
[14]N. Glendenning and J. Rafelski, Phys. Rev. C **31**, 823 (1985).
[15]A. Shor, Phys. Rev. Lett. **54**, 1122 (1985).
[16]J. Randrup and C. M. Ko, Nucl. Phys. **A343**, 519 (1980).
[17]K. H. Muller, Nucl. Phys. **A395**, 509 (1983).
[18]F. Asai, H. Sato, and M. Sano, Phys. Lett. **98B**, 19 (1981).
[19]T. S. Biro, B. Lukacs, J. Zimanyi, and H. W. Barzm, Nucl. Phys. **A386**, 617 (1982).
[20]C. Derreth, W. Greiner, H. T. Elze, and J. Rafelski, Phys. Rev. C **31**, 1360 (1985).
[21]F. Ochiai, Y. Yoshimura, M. Chikawa, N. Fujiwara, M. Fukawa, H. Kichimi, E. Kohriki, O. Kusumoto, J. MacNaughton, K. Miyano, S. Noguchi, Y. Noguchi, T. Okusawa, A. Ono, T. Sato, R. Sugahara, A. Suzuki, K. Takahashi, and S. Yamashita, Z. Phys. C **23**, 369 (1984).
[22]S. Noguchi, N. Fujiwara, M. Chikawa, M. Fukawa, H. Kichimi, E. Kohriki, O. Kusumoto, J. MacNaughton, K. Miyano, Y. Noguchi, F. Ochiai, T. Okusawa, A. Ono, T. Sato, R. Sugahara, A. Suzuki, K. Takahashi, S. Yamashita, and Y. Yoshimura, Z. Phys. C **24**, 297 (1984).
[23]K. Miyano, Y. Noguchi, M. Fukawa, E. Kohriki, F. Ochiai, T. Sato, A. Suzuki, K. Takahashi, Y. Yoshomura, N. Fujiwara, S. Noguchi, S. Yamashita, and A. Ono, Phys. Rev. Lett. **53**, 1725 (1984).
[24]H. Reinhardt, B. V. Dang, and H. Schulz, Phys. Lett. **159B**, 166 (1985).
[25]S. Banerjee, S. N. Ganguli, P. K. Malhotra, and R. Raghavan, Nucl. Phys. **B150**, 119 (1979).
[26]K. Heller, O. E. Overseth, G. Bunce, F. Dydak, and H. Taureg, Phys. Lett. **68B**, 480 (1977).
[27]K. Heller, P. T. Cox, J. Dworkin, O. E. Overseth, P. Skubic, L. Schachinger, T. Devlin, B. Edelman, R. T. Edwards, G. Bunce, R. Handler, R. March, P. Martin, L. Pondrom, and M. Sheaff, Phys. Rev. Lett. **41**, 607 (1978).
[28]U. Camerini, D. Cline, and N. Seghal, Nucl. Phys. **B33**, 505 (1972).
[29]B. Y. Oh and G. A. Smith, Nucl. Phys. **B40**, 151 (1982).
[30]M. A. Mandelkern, L. R. Price, J. Schultz, and D. W. Smith, Phys. Rev. D **27**, 19 (1983).
[31]S. J. H. Parkin, S. N. Tovey, and J. W. Wignall, Nucl. Phys. **B277**, 634 (1986).
[32]J. Cugnon and J. Vandermaeulen, Phys. Lett. **146B**, 16 (1984).
[33]M. Kohno and W. Weise, Phys. Lett. B **179**, 15 (1986).
[34]W. R. Gibbs, in *Intersections Between Particle and Nuclear Physics (May 26–31, 1986, Lake Louise, Canada),* Proceedings of the Second Conference on the Intersections of Particle and Nuclear Physics, AIP Conf. Proc. No. 150, edited by Donald F. Geesaman (AIP, New York, 1986), p. 505.
[35]C. M. Ko and R. Yuan, Phys. Lett. B **192**, 31 (1987).
[36]S. Nagamiya, Phys. Rev. Lett. **49**, 1383 (1982).